J Mol Model (2010) 16:993–1002
DOI 10.1007/s00894-009-0601-3

ORIGINAL PAPER

Selectivity of Imidacloprid for fruit fly versus rat nicotinic acetylcholine receptors by molecular modeling

Gen-Yan Liu · Xiu-Lian Ju · Jin Cheng

Received: 9 August 2009 / Accepted: 26 September 2009 / Published online: 29 October 2009

Abstract For better understanding of the mechanisms of selective binding of the representative nicotinic acetylcholine receptor (nAChR) agonist neonicotinoid Imidacloprid (IMI), three-dimensional models of fruit fly α1β2 and rat α4β2 nAChRs were generated by homology modeling, using the crystal structure of the acetylcholine-binding protein (AChBP) of *Lymnaea stagnalis* and the nAChR of *mus musculus* as the templates, respectively. The conformational stability of the two models was studied by molecular dynamics (MD) and the quality of the models was confirmed. Especially, insecticide Imidacloprid was docked into the putative binding site of the fruit fly α1β2 and rat α4β2 nAChRs by Surflex-docking. The calculated docking energies were in agreement with the experimental data and the putative binding sites were also consistent with the results from labeling and mutagenesis experiments. Furthermore, the mechanisms of Imidacloprid selectively acting on fruit fly versus rat nAChRs were discussed.

Keywords Fruit fly α1β2 nAChR · Homology modeling · Imidacroprid · Molecular docking · Rat α4β2 nAChR

Introduction

The nicotinic acetylcholine receptor (nAChR) is a member of the cys-loop superfamily of pentameric ligand-gated ion channels (LGICs), which also include serotonin type 3 receptors (5-HT_3), γ-aminobutyric acid ($GABA_A$ and $GABA_C$) and glycine receptors [1–4]. Each of these LGICs forms homo- or hetero- pentamers of related subunits [1, 2]. However, like other LGICs only a limited number of naturally occurring functional nAChR structures have been identified to date [5].

Vertebrate nAChRs consists of diverse subtypes assembled as five subunits in combinations from ten α (α1-10), four β (β1-4), γ, δ, and ε subunits. The skeletal muscle type, with stoichiometry (α1)2β1γδ, is the major neurotransmitter receptor at the neuromuscular junction [6, 7]. The neuronal nAChRs are found in the nervous system and comprise five α subunits (*e.g.*, α7, α9) or a combination of α and β subunits (*e.g.*, α4β2, α3β4α5). Specially, α4β2 receptor consisted of two α4 and three β2 subunits is the most abundant subtype in brain and represents more than 90% of the [^{3}H]nicotine binding sites [8–11] (Fig. 1).

Insect nAChRs are less well understood than their vertebrate counterparts as to functional architecture and diversity (Fig. 1). They are widely distributed in the synaptic neuropil regions of the insect central nervous system (CNS) [12]. Genes encoding the ligand-binding α and structural β subunits have been cloned in several insect species. In the fruit fly (*Drosophila melanogaster*), seven α (Dα1-7) and three β (Dβ1-3) subunit genes are cloned [13–15]. However, heterologous expression of fruit fly nAChRs has so far been unable to directly examine the interactions between α and β subunits that must exist *in vivo* and no reports of *in vitro* expression of a fully functional nAChR have been published for fruit fly [16]. Recently, most information about the functionality of insect subunits has come from studies in which α-subunits were co-expressed with a vertebrate β-subunit, or N-terminal regions were fused with C-terminal regions of 5-HT_3 genes [17–19]. However, these hybrid receptors do not faithfully reflect native insect nAChRs. Immunology approaches suggest

G.-Y. Liu · X.-L. Ju (✉) · J. Cheng
Key Laboratory for Green Chemical Process of Ministry of Education, School of Chemical Engineering & Pharmacy, Wuhan Institute of Technology,
Wuhan 430073, People's Republic of China
e-mail: xiulianju2001@yahoo.com

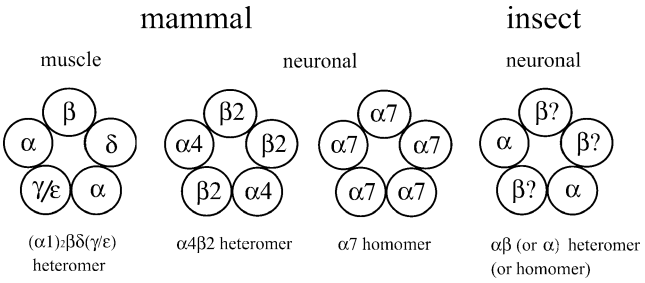

Fig. 1 Functional assembly of mammalian and insect nicotinic receptor subtypes consisting of different subunit combinations viewed in cross-section from the top

two native fruit fly subtypes consisting of Dα1/Dα2/Dβ2 and Dα3/Dβ1 [13, 20, 21]. Other genes encoding insect nAChR subunits are known from peach aphid (*Myzus persicae*), migratory locust (*Locusta migratoria*), tobacco hornworm (*Manduca sexta*), honey bee (*Apis mellifera*), desert locust (*Schistocerca gregaria*), and *et al*., although their diversity and native structures are not clarified [13, 14, 22–24].

Each of vertebrate and insect nAChR subunits possesses an N-terminal extracellular ligand-binding domain (LBD) with a conserved di-cysteine loop, four transmembrane regions (TM1-TM4), and a large intracellular loop between TM3 and TM4. The LBDs, which are around 210 amino acid residues long, bear ligand-binding sites for agonists and competitive antagonists [25]. The binding sites are located at the LBD interface and formed by loops A, B, and C of the α subunit and loops D, E, and F which are normally located at α or non-α subunit [4, 10, 25–28].

Numerous laboratories have focused on the structure and function of nAChRs for more than a decade [29]. Firstly, the electron microscopic analyses of nAChRs from the *Torpedo marmorata* electric ray organ have been reported, which have produced a picture of the intact channel, revealing the overall organization of the pentameric assembly, the architecture of the LBD and the pore region of each subunit [30, 31]. Secondly, the acetylcholine-binding protein (AChBP) from snail (*Lymnaea stagnalis*) was discovered in glial cells as a nonchannel homolog of the extracellular domain of nAChRs [3, 32]. AChBP shares 25% sequence identity with nAChRs and has the same pentameric assembly. Subsequently, X-ray crystal structures of Ls-AChBP homologs from *Aplysia californica* (Ac-AChBP) and *Bulinus truncatus* (Bt-AChBP) were reported [33, 34]. In recent years, several crystal structures of AChBPs have been solved in different bound states, providing atomic-resolution details of the interactions between the LBD and a variety of agonists and antagonists [3, 25, 33, 35–38]. For mammals, none but a crystal structure of the extracellular domain of the mouse (*mus musculus*) nAChR α1 subunit bound to α-bungarotoxin was determined at 1.94 Å resolution [29]. It should be noticed that all the six regions (loops A-F) that make up the ligand binding site are highly conserved in both AChBPs and nAChR subunits. Thus the crystal structures of mollusk AChBPs complexed with agonist Imidacloprid, as structural surrogates of the nAChR extracellular ligand-binding domain, provide substantial information on the recognition properties of the neonicotinoid binding site [3, 25, 35].

Neonicotinoids, such as Imidacloprid, are extensively used for pest management and have become an important class of insecticides [13, 39]. The safety and effectiveness of neonicotinoids has been attributed, at least in part, to the high selectivity of these compounds for insect compared to mammalian nAChRs [13, 14, 40]. High affinity Imidacloprid binding sites are found in nervous system membrane preparations from insects of many orders, and radioligand binding assays and electrophysiological studies show that insect synaptic and cell body nAChRs are targeted by neonicotinoids [41, 42].

To understand the mechanisms of the selective binding of nAChRs agonist Imidacloprid to insect over mammalian nAChRs may assist in the development of safe and effective insecticides. In the present study, the LBD of fruit fly α1β2 and rat α4β2 nAChRs were built by the homology modeling, using the crystal structure of the acetylcholine-binding protein (AChBP) of *Lymnaea stagnalis* and the nAChR of *mus musculus* as the templates, respectively. These models were optimized and validated by computational tools as well as by comparison with experimental results. Especially, neonicotinoid Imidacloprid was docked to the binding sites of fruit fly α1β2 and rat α4β2 nAChRs, respectively, and the results may be used to explain and consolidate experimental data. Meanwhile, the mechanisms of Imidacloprid selectively acting on the fruit fly versus rat were studied.

Methodology

Sequence alignment and homology modeling

All calculations containing homology modeling and surflex-docking studies were performed using SYBYL software package version 7.3 (http://www.tripos.com/) running on Linux workstation [43].

The sequences of the fruit fly α1 (P09478), β2 (P25162) and rat α4 (P09483), β2 (P12390) were obtained from TrEMBL/Swiss-Prot databank. These four sequences were all edited to remove four transmembrane regions (TM1-TM4) and a large intracellular loop between TM3 and TM4.

Template selection is an important starting point in homology modeling because the template directly determines the main folding of the target structures, and

influences their quality. Due to technological limitations of the membrane-bound protein crystallization, few well-resolved structures of membrane-bound proteins have been obtained through X-ray crystallography or NMR methods. Recently, Ihara *et al*. reported a high resolution crystal structure of AChBP complex (PDB entry: 2ZJU, 2.58 Å resolution) from the snail *Lymnaea stagnalis* with neonicotinoid insecticides Imidacloprid [25]. We chose this protein as a template to build the homology model of fruit fly α1 and β2 subunits. However, because of the low sequence identity between Ls-AChBP and rat nAChR subunits, the LBD of the mouse α1 subunit of the nAChR (PDB entry: 2QC1, 1.94 Å resolution) was chosen as a template to build the homology model of the rat α4 and β2 subunits [29].

Each subunit was built using the following procedure. After aligning each target sequence with the template sequence using the Needleman and Wunsch method, a multiple sequence format (MSF) file was generated [44]. The sequences and structures are structurally aligned using ORCHESTRAR program of the BATON method [45]. All target peptide chains were built by recognizing the structure conserved regions (SCR), searching the gaps and adding the side chains.

Model assembly and molecular dynamics

The fruit fly $(\alpha1)_2(\beta2)_3$ and rat $(\alpha4)_2(\beta2)_3$ pentamers were generated by aligning the independently produced monomer model onto the protomer of Ls-AChBP. Two α and three β subunits were superimposed onto the 2ZJU structure using biopolymer to generate a pentameric assembly in a counterclockwise configuration of (α)(β)(α)(β)(β) for both fruit fly $(\alpha1)_2(\beta2)_3$ and rat $(\alpha4)_2(\beta2)_3$ nAChRs. This method allowed the structures of two α and three β subunits to be identical within their own types in the model.

Both of the obtained pentamer models were optimized energetically using AMBER7 FF99 force field by performing a conjugate gradient minimization with 10,000 step iterations to reach a root-mean-square (RMS) gradient energy of 0.5 kcal mol^{-1} $Å^{-1}$. Subsequently, in order to determine whether the LBD structures of fruit fly $(\alpha1)_2(\beta2)_3$ and rat $(\alpha4)_2(\beta2)_3$ nAChR are stable, molecular dynamics (MD) simulations were performed on both of the modeled receptors over 500 ps with the step size of 1 fs at a constant temperature 300 K [43].

Ligand docking

To validate the 3D homology models, the Imidacloprid was docked into the putative binding pocket of fruit fly $(\alpha1)_2(\beta2)_3$ and rat $(\alpha4)_2(\beta2)_3$ nAChRs. Before performing ligand docking, it is critical to search for the binding pocket of the prepared protein. In this study, Ligand mode was adopted to generate the protomol in the program Surflex-dock for fruit fly $(\alpha1)_2(\beta2)_3$ nAChR and Residue mode was adopted to generate the protomol for rat $(\alpha4)_2(\beta2)_3$ nAChR. Ligand mode was applicable to the receptor containing a ligand in the same coordinate space and residue mode defines the active site by considering a reasonable distance around chosen residues [43]. In addition, two parameters that can significantly affect the size and extent of the protomol generated are the threshold and the bloat values.

Surflex-Dock uses an empirical scoring function and a patented search engine to dock ligands into a binding site of protein. In terms of docking accuracy, Surflex-Dock 2.1 performs as well as the best available methods [46]. The scoring function, which is based on the binding affinities of protein-ligand complexes, takes into account several terms, including hydrophobic, polar, repulsive, entropic, and salvation [47]. The total docking scores are expressed in $-\log_{10}K_d$ units to evaluate the docking results, where K_d represents a dissociation constant of a ligand. In present study, the binding free energies (kcal mol^{-1}) of protein-ligand complexes would be obtained according to the calculation as follows, where RT=0.59 kcal mol^{-1}:

$$\text{Free Energy of Binding} = RT\log_e K_d \quad (1)$$

Results and discussion

Sequences alignment

The details of the alignment are shown in Fig. 2. The sequence identity percentage between the extracellular domain of insect nAChR subunits and the AChBP is about 25%, but the second structure similarity of both was estimated as close to 80%. Therefore, AChBP is a suitable 3D-structure template for the ligand-binding domain of insect nAChR α and β subunits. Additionally, the identity percentages of the sequences of rat α4 and β2 nAChR subunits with mouse α1 subunit are 44% and 38%, respectively.

Sequence alignment (Fig. 2) revealed most of the amino acid residues within the binding pockets of the AChBP, fruit fly a1β2 and rat a4β2 nAChRs are the same or quite similar except loop D and loop E. The residues involved in binding sites in all homology models are listed in Table 1. The Ls-AChBP pentamer has five ligand-binding pockets. Each binding pocket is formed in a cleft made of loops A-F, part of the principal subunit interface [(+)-chain)], a series of β-strands, and part of the complementary adjacent

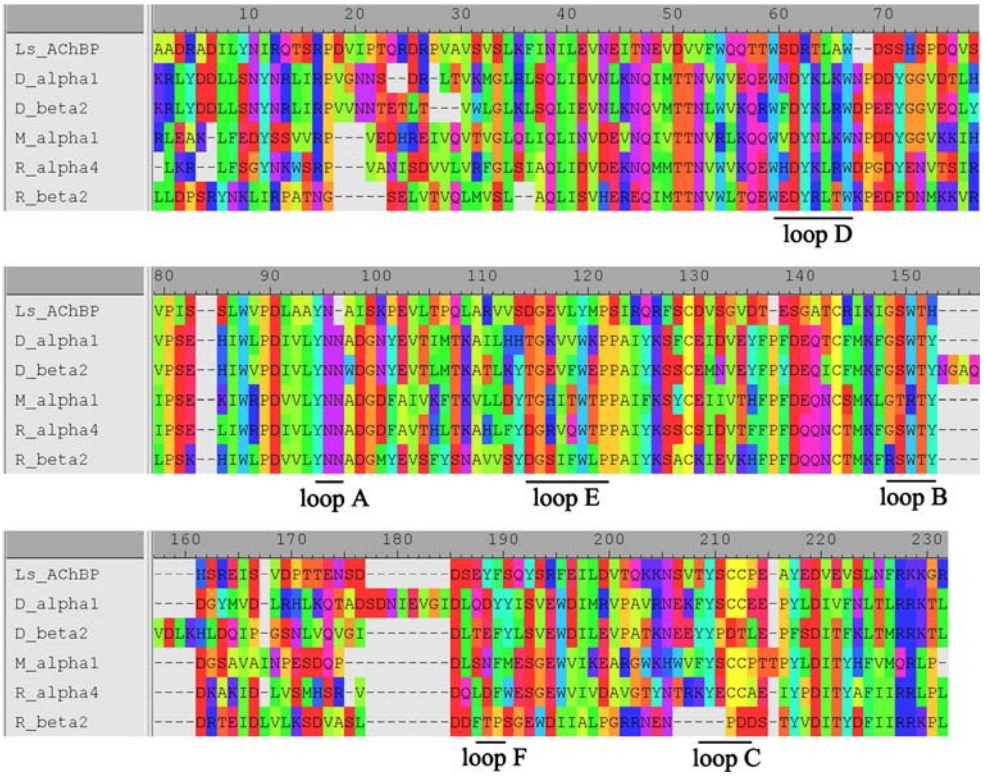

Fig. 2 Each target sequence (the ligand-binding domain of fruit fly α1, β2 and rat α4, β2 nAChR subunits) was aligned with that of Ls-AChBP. Different types of amino acids are painted in different colors

subunit interface [(-)-chain]. Based on these amino acids of interface, a cavity with a bottom (the (+)-chain of Tyr89, Tyr185, the (-)-chain of Tyr164, Trp53), a top (Arg104, Leu112) and walls (Trp143, double Cys187, 188, Tyr192, the (+)-chain closed to His145, the (-)-chain of Met114, Gln55,) are formed [3, 48].

Build homology modeling

In mammals, nAChRs play crucial roles in neuromuscular and inter-neuronal cholinergic neurotransmission. The mammalian $(\alpha4)_2(\beta2)_3$ nAChR, consisting of two α4 and three β2, is the most abundant and widespread in brain and is a major target for potential therapeutic agents for neuropathic diseases, cognitive enhancement, analgesia, and smoking cessation and is also important in considering the selective toxicity of insecticides. The toxicity of neonicotinoid to mammals is considered to be primarily due to action at the α4β2 nAChR in brain based on the centrally mediated toxicity signs or behaviors as well as the agonist action [14].

For insect, nAChRs are widely distributed in the insect central nervous system (CNS) as the important targets for insecticide action, although the native nAChR subtype is not clear [24]. In fruit fly, when any of the four α subunits is coexpressed with vertebrate β subunits, [^{3}H]Imidacloprid binding is clearly observed. Heterologous expression of any *Drosophila* α subunit with a vertebrate β subunit constitutes the available hybrid receptors at present. Two native *Drosophila* subtypes consisting of Dα1/Dα2/Dβ2 and Dα3/Dβ1 have been determined by immunological approaches [13, 20, 21]. Meanwhile, a lot of protein biochemical approaches to native *Drosophila* nAChR subunits, reveal the existence of several subunits, including Dα2 as the main neonicotinoid-binding component [12]. Thus, two representative models of fruit fly $(\alpha1)_2(\beta2)_3$ and rat $(\alpha4)_2(\beta2)_3$ have been constructed to study the selective action mechanism of neonictionoid insecticides Imidaclo-

Table 1 Residue homology between AChBP and the different nicotinic subtype models at the level of the 3D-structure

Model	α-subunit						β-subunit					
AChBP	Tyr89	Trp143	Tyr185	Cys187	Cys188	Tyr192	Trp53	Gln55	Thr57	Leu112	Met114	Pro115
F_α1β2	Tyr89	Trp145	Tyr195	Cys197	Cys198	Tyr202	Trp51	Lys53	Arg55	Phe113	Glu115	Pro116
R_α4β2	Tyr86	Trp142	Tyr183	Cys185	Cys186	Tyr190	Trp47	Thr49	Glu51	Phe109	Leu111	Pro112

prid between insects and mammals. The final two models are respectively given in Fig. 3a and b.

Conformational analyses

Two repeating torsion angles along the backbone chain, which are called Φ and Ψ, are used to describe the conformations of the models. By comparing the Φ and Ψ dihedral angles of the homology models to the statistical Ramachandran map obtained from ProTable program, evaluation of the backbone conformation of the constructed model and detection of dissatisfactory residues is straightforward [18].

Conformationally unreasonable residues fall in the disallowed regions of the statistical Ramachandran map. Glycine residues often locate at the disallowed regions. As the structure of glycine residue contains two hydrogen atoms at α-position, one hydrogen atom in the side chain possesses an extremely small van der Waals radius and was more unrestricted than the other residues. Figure 4a indicates that approximately 98.53% of the residues in the fruit fly α1β2 nAChR model are either in the most accepted or in the additionally accepted regions of the Ramachandran plot. Figure 4b shows that 98.86% of residues in the rat α4β2 nAChR model are located in the satisfactory regions. In Fig. 4a and b, most residues converge around a Φ value of -135° and a Ψ value of +135°, which agrees well with the fact that two models are mainly made up of β-sheets. Accordingly, the two constructed models are conformationally reasonable and can be used for further studies.

Molecular dynamics

The two obtained pentamer were submitted to the described minimization and MD protocol to assess their stability, and the results were shown in Fig. 5a and b, the structures of fruit fly $(\alpha1)_2(\beta2)_3$ and rat $(\alpha4)_2(\beta2)_3$ nAChRs deviated rapidly from the initial structure within the first 100 ps of the MD simulation, but after about 300 ps, the total root-mean-square deviation (RMSD) of the backbone atoms of the fruit fly $(\alpha1)_2(\beta2)_3$ and the rat $(\alpha4)_2(\beta2)_3$ models stabilized at around 4.5 Å, suggesting that a 500 ps unrestrained simulation was sufficient for stabilizing a fully relaxed model and the core structures of the two proteins were stable during the MD simulation. Moreover, comparison of the structures at different times of MD simulation with the starting structure revealed no major changes in overall conformation.

Additionally, Fig. 5c (fruit fly model) and d (rat model) displayed that the total potential energy *vs*. time collected per 1 ps during the entire 500 ps MD simulation. Obviously, the total energies of two models kept to equilibrate after 200 ps. Therefore, the obtained results suggested that the two models are reliable and can be used for subsequent study.

Binding free energies

Considering that the receptor was a transmembrane channel, the protomol was defined by setting the threshold and the bloat values to 0.5 and 0 Å, respectively. The representative neonicotinoid insecticide Imidacloprid, which has been prevalently applied as a highly efficient insecticide in agriculture, was chosen as the docked ligand to validate the quality of the homology models of rat α4β2 and fruit fly α1β2 nAChRs. From Table 1, we found that the residues of Loops A-F were highly conversed in two obtained models. Thus similar cavities of rat α4β2 and fruit fly α1β2 nAChRs located at the α(+)/β(−) subunit interface have been explored for binding sites using two different modes to search for the binding pocket.

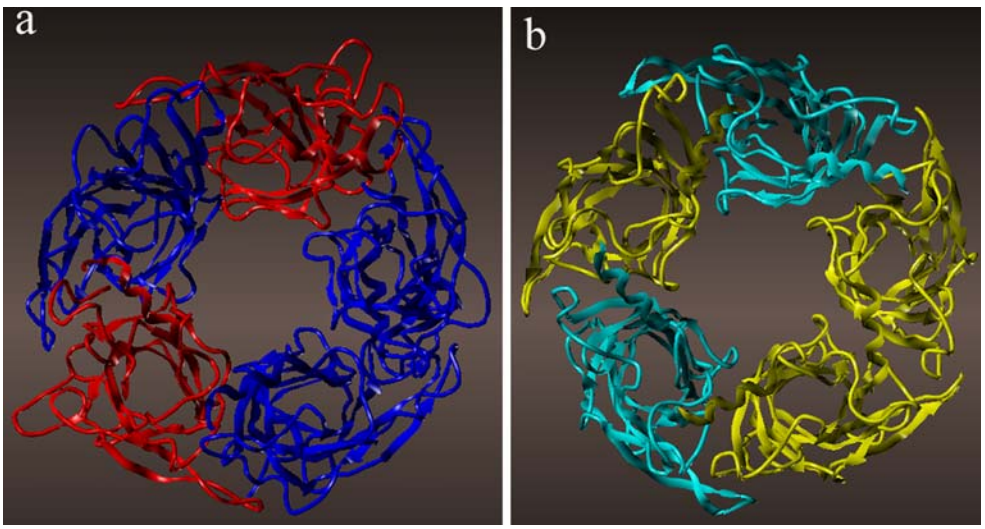

Fig. 3 The ligand-binding domain of nAChR viewed from N- to C-terminal (**a**: fruit fly α1β2 and **b**: rat α4β2). Five subunits were shown in Ribbon/Tube representation, with the model comprising two α subunits, three β subunits, where α1 subunit was in red, β2 (fruit fly) in blue, α4 in cyan, β2 (rat) in yellow

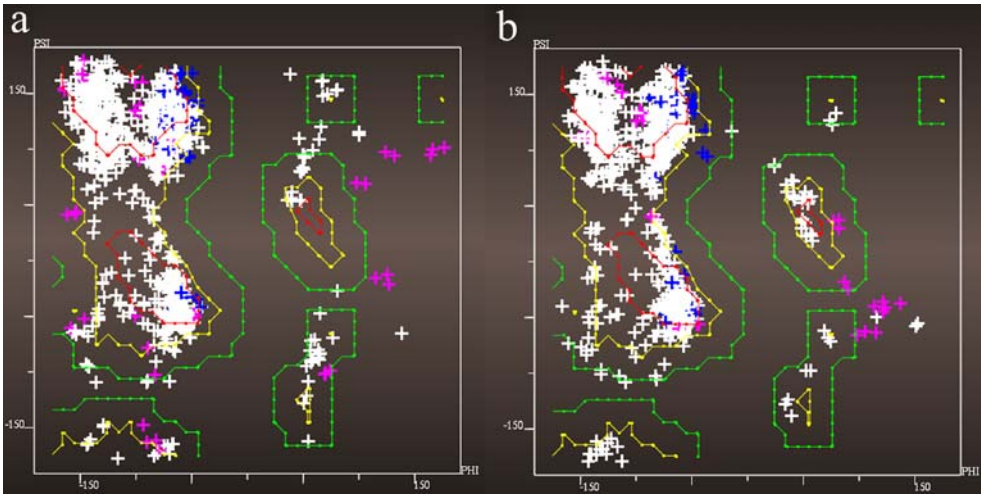

Fig. 4 Φ-Ψ Graph of the backbone of fruit fly $(\alpha1)_2(\beta2)_3$ (**a**) and rat $(\alpha4)_2(\beta2)_3$ (**b**) nAChR. The conformationally disfavorable residues were labeled. (blue: proline residues; magenta: glycine residues; white: all other residues. red: core regions; yellow: allowed regions; green: generous regions; all else: disallowed regions)

Using Surflex-docking, Imidacloprid was docked to the fruit fly α1β2 and rat α4β2 nAChRs, and the calculated binding free energies of five top-scoring poses were listed in Table 2. All RMS deviations were calculated based on the best docked pose (IMI01) over all five dockings. From Table 2, the docked complexes of fruit fly α1β2 were more stable because all conformations of ligands have the lower binding free energies and the RMS deviations in fruit fly α1β2 model than in rat α4β2 model. The highest calculated binding free energies of protein-ligand com-

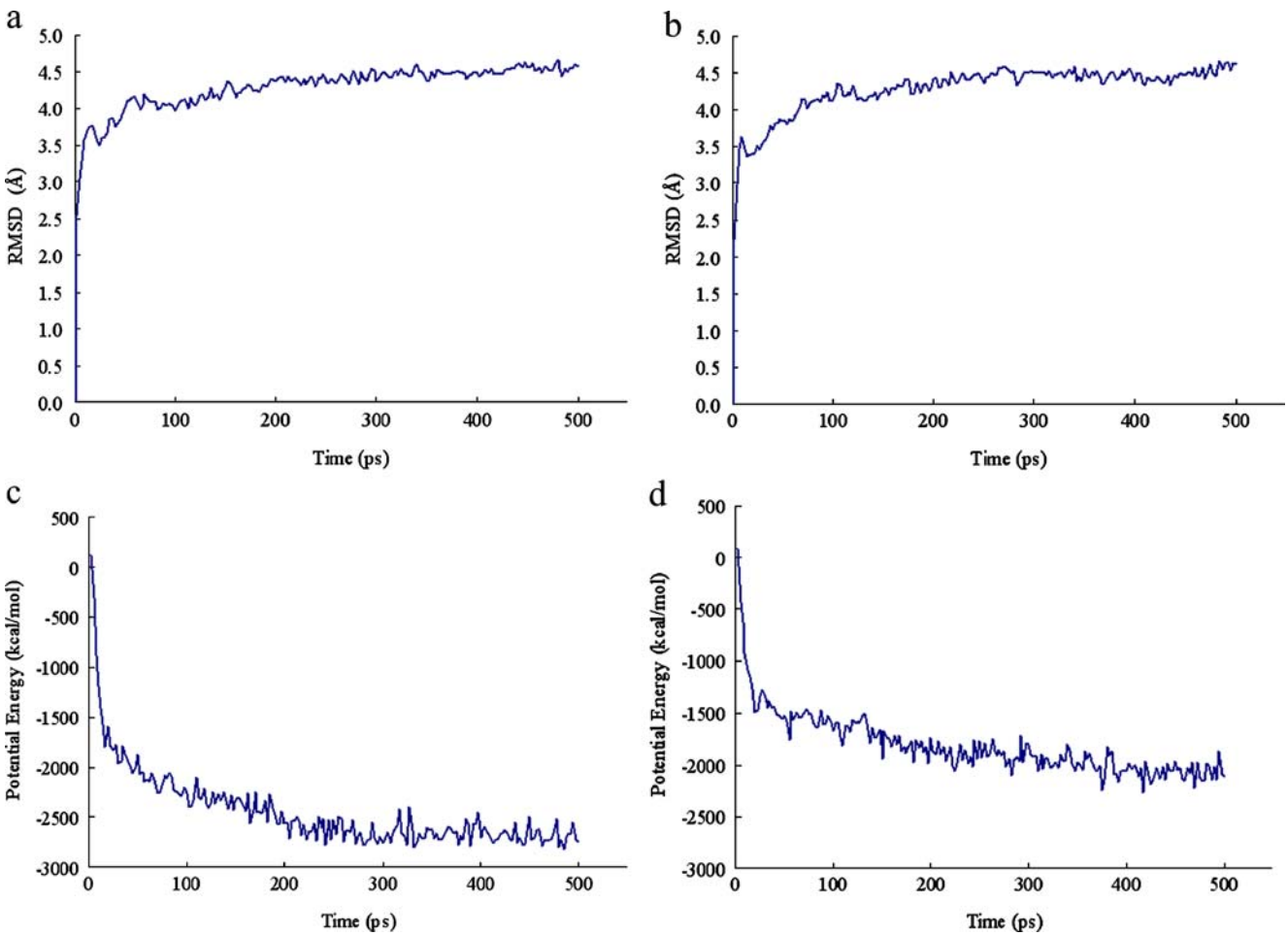

Fig. 5 Plot of all backbone atoms root mean square deviations (RMSD) of the constructed models over 500 ps molecular dynamics (MD) simulation using the best initial model as a reference: **a:** fruit fly $(\alpha1)_2(\beta2)_3$ and **b:** rat $(\alpha4)_2(\beta2)_3$. Plot of the total potential energy versus the simulation time. **c:** fruit fly $(\alpha1)_2(\beta2)_3$ and **d:** rat $(\alpha4)_2(\beta2)_3$

Table 2 The binding free energies and RMSD of top-scoring conformations of surflex-docking

Top-scoring conformation	Fruit fly model			Rat model		
	Cscores	Binding free energies	RMSD	Cscores	Binding free energies	RMSD
IMI01	4.60	-6.25	0.00	3.26	-4.43	0.00
IMI02	4.39	-5.96	0.15	2.94	-3.99	1.58
IMI03	4.27	-5.80	0.28	2.68	-3.64	0.80
IMI04	4.19	-5.69	1.20	2.43	-3.30	0.75
IMI05	4.17	-5.67	0.20	2.41	-3.27	0.91

plexes of fly α1β2 and rat α4β2 models were -6.24 kcal mol^{-1} and -4.43 kcal mol^{-1}, respectively. These results demonstrated that the binding-site specificity of fruit fly versus rat was greater for Imidacloprid, which was in agreement with the IC_{50} values of Imidacloprid binding to fruit fly nAChRs (IC_{50}=4.6 nM) and rat nAChRs (IC_{50}= 2600 nM) [49, 50].

Binding mode for Imidacloprid

The mechanism of the selective binding of Imidacloprid to rat α4β2 and fruit fly α1β2 nAChRs was further explored with Surflex-docking, and the binding modes are shown in Fig. 6. As illustrated in Fig. 6a and b, Surflex-docking analyses clearly show that Imidacloprid fitted into the putative binding pockets located at the α(+)/β(−) subunit interface. Specially, all the residues composition of the binding sites (Fig. 7) retained very small RMSD values during the MD simulations. The low RMSD fluctuation (1.5 Å) and structural comparison along with the simulation time indicate that, as expected, the starting binding site represents a stable conformation. Additionally, the RMSD for rat α4β2 nAChR from the initial structure (Fig. 7b) is slightly larger than that for the fruit fly α1β2 nAChR (Fig. 7a).

Figure 6c and d show the detailed binding mode between Imidacloprid and the active sites of rat α4β2 and fruit fly α1β2 nAChRs, respectively. H-bonds are also introduced to help understand the interactions of the complexes, which allowed us to determine the amino acid residues involved in the recognition of nAChR agonists. The distances and angles of H-bonds are given in Table 3. According to the docking and MD results, it can be speculated that Imidacloprid has higher potency toward fruit fly nAChR than rat nAChR.

As seen in Fig. 6c, Imidacloprid mainly interacted with loop C segments from the (+)-chain in rat α4β2 homology model. Shimomura *et al*. have found that replacement by glutamate of the proline in loop C of the *Drosophila* Dα2 subunit reduces the Imidacloprid sensitivity of the Dα2β2 hybrid nAChR, whereas its reverse mutation in the α4β2 nAChR enhanced sensitivity [51]. This conclusion suggested that the loop C residues contributed to the neonicotinoid sensitivity of nAChRs. Similarly, in our docked-complex, the nitrogen atom of the pyridine ring formed a hydrogen bond with the side chain of Tyr183 corresponding to Tyr185 of Ls-AChBP in loop C and the oxygen atom of the side chain of Tyr190 corresponding to Tyr191 of Ls-AChBP in loop C formed a hydrogen bond with the guanidine moiety of Imidacloprid. The pyridine ring was also found to stack with the aromatic ring of Trp142 in the rat α4β2 model, which was similar with the Ls-AChBP-Imidacloprid complex [25]. From the MD simulation of the rat α4β2 model, the residue Trp142 of loop B, the Tyr183 of loop C, and the Tyr190 of loop C have not showed a significant shift, although these residues moved towards the inside of the binding cavity slightly. A similar shift of Trp142 and Trp190 of rat α4β2 nAChR in the middle of the binding site was also observed by Bisson *et al*. [48]. Thus, the results suggested that the observed interactions of the binding sites with Imidacloprid were reasonable and stable.

Interestingly, we noticed that the nitro group of Imidacloprid was far from the anionic residue Glu51 of loop D and did not interacted with any residues of loop D (Fig. 6c). Most of mammalian nAChRs are likely to show reduced sensitivity to neonicotinoids due to the lack of the basic cationic residues in loop D. Shimomura *et al*. have demonstrated the fact that the negative electrostatic force of Glu51 was postulated to interfere electrostatically with the neighboring basic or neutral residue-neonicotinoid interactions, thereby reducing the neonicotinoid sensitivity of nAChRs containing the β2 subunits [52]. In complete contrast, the positively charged amino acid Lys53 of the fruit fly model corresponding to Gln55 of Ls-AChBP interacted electrostatically with the nitro group of Imidacloprid and formed a hydrogen bond with oxygen and nitrogen atoms of nitro group, respectively (Fig. 6d). We also observed the Lys53 showed much smaller fluctuations compared with the other binding site residues during MD simulation. Consistent with this hydrogen bond, the similar hydrogen bond between Gln55 and the nitro group were

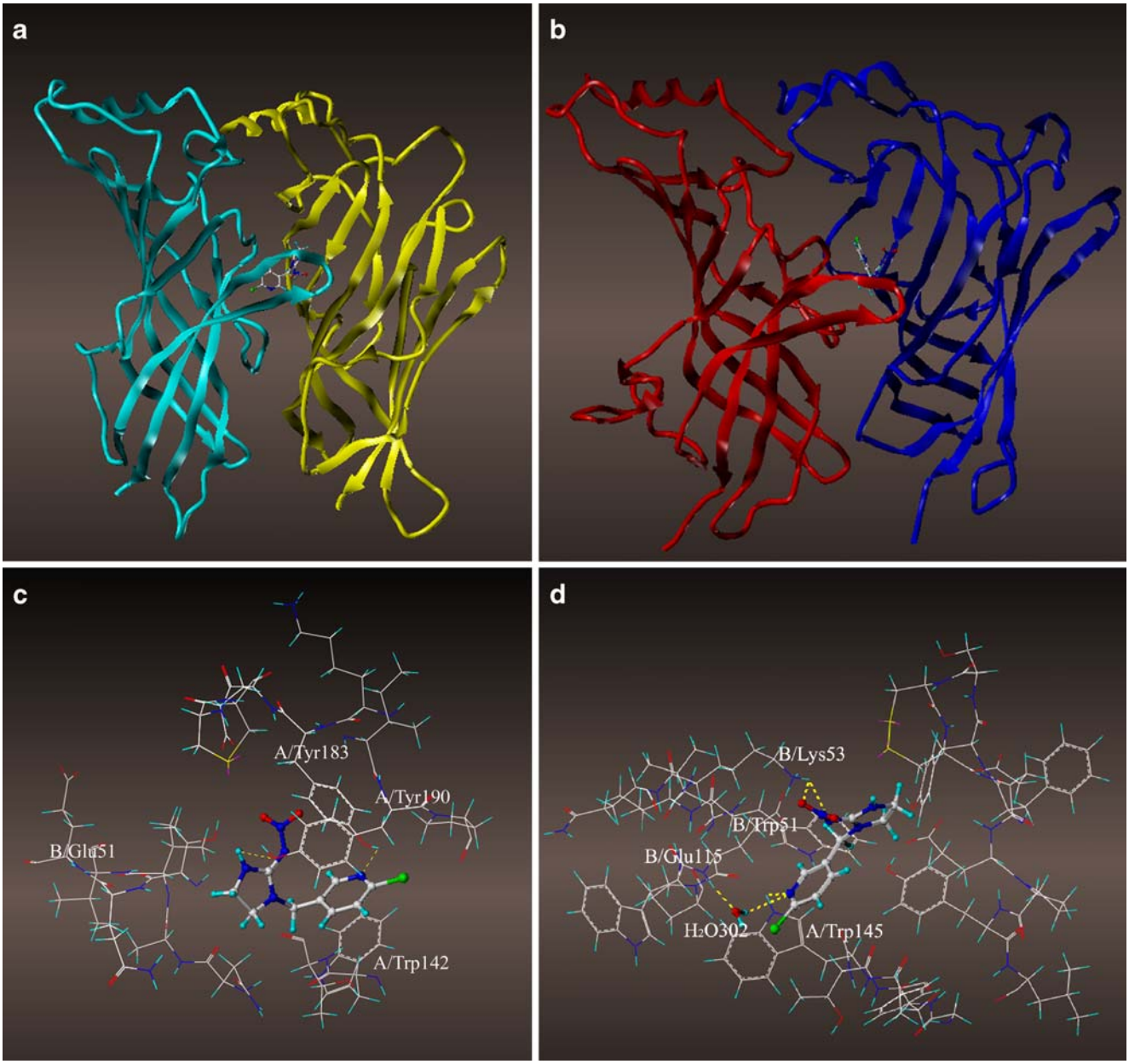

Fig. 6 Ligand binding analyses based on the refined homology model: **a** a ribbon representation of rat α4/β2 dimer with Imidacloprid. Cyan: α4 subunit, Yellow: β2 subunit; **b** a ribbon representation of fruit fly α1/β2 dimer with Imidacloprid. Red: α1 subunit, Blue: β2 subunit; **c** a detailed view of the binding site and hydrogen bonds of rat α4β2 nAChR with Imidacloprid; **d** a detailed view of the binding site and hydrogen bonds of fruit fly α1β2 nAChR with Imidacloprid. The detailed hydrogen bonds were depicted by yellow dotted line

observed in both Ls-AChBP-Imidacloprod complex and Ac-AChBP-Imidacloprid complex [25, 35]. Tomizawa and Casida have reported that the critical feature of Imidicloprid for insect nAChR binding appears to be the negatively charged tip or region of the nitro group [13, 14]. Ihara *et al*. also have found that the loop D of the nAChRs binding site is likely to be involved in the direct interactions with the nitro or cyano group of neonicotinoids [53]. However, as our docked results, the rat α4β2 model possessed a negatively charged amino acid Glu51 in loop D and it interfered electrostatically with the neighboring Trp49 residue interacted with Imidacloprid. To sum up, a lysine (or alternatively arginine or histidine) cationic residue in loop D interacted with the negatively charged nitro tip of Imidacloprid is important in selectivity for insect versus mammalian nicotinic receptors.

As seen in Fig. 6d, when Imidacloprid was docked with fruit fly α1β2 model, the pyridine ring of Imidacloprid interacted with loop B segments from the (+)-chain and loop E segments from the (-)-chain. The nitrogen atom of

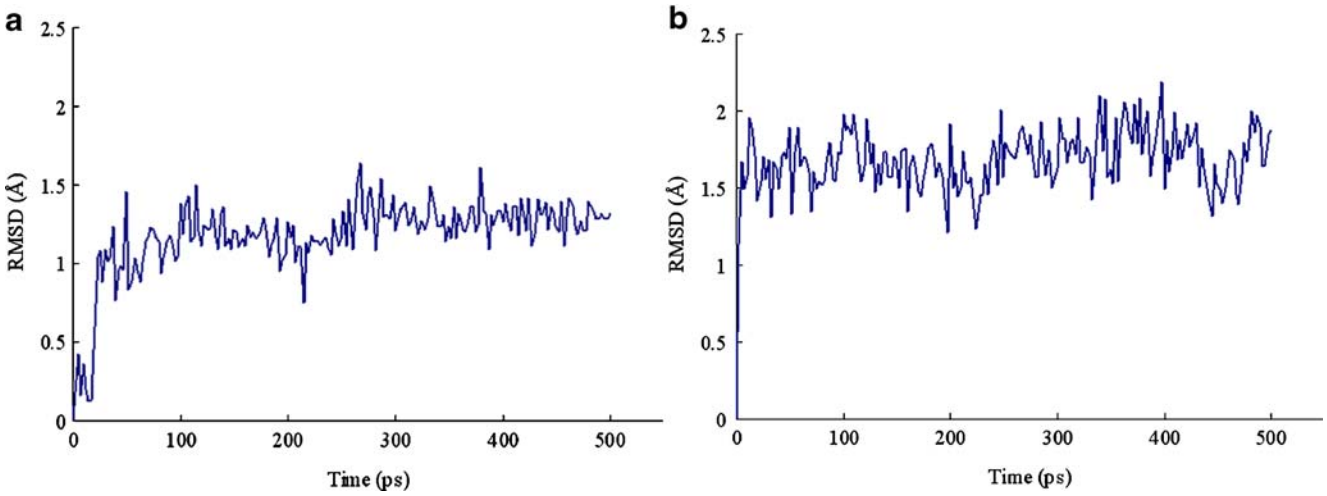

Fig. 7 Plot of RMSD of the binding site residues versus the MD simulation time. **a:** fruit fly $(\alpha1)_2(\beta2)_3$ and **b:** rat $(\alpha4)_2(\beta2)_3$

the pyridine ring formed a hydrogen bond with the main chain of Glu115 in loop E *via* a water molecule (H_2O 302), resembling the observations for both the Ls-AChBP-Imidacloprid complex [25] and Ac-AChBP-epibatidine complex [38]. In recent studies, the water-bridge formation has been validated to enhance the binding or stabilize the receptor-ligand binding nAChR complexes [54]. Hence, we used two water molecules to fill the similar cavity positions at the binding sites of the fruit fly α1β2 and rat α4β2 nAChRs and the new structures were energy-minimized prior to the molecular docking. The water-bridge was found in fruit fly α1β2 model while not in rat α4β2 nAChRs, implying that the hydrogen bond bridged by water molecule possibly enhance the affinity of Imidacloprid for insect nAChRs.

Specially, we noticed that the nitrogen atom of the pyridine ring also formed a hydrogen bond with the side chain of Trp145 corresponding to Trp143 of Ls-AChBP in loop D. This result is also similar with the Ls-AChBP-clothianidin and Ac-AChBP-epibatidine complexes [25, 38]. The chlorine atom was located in the vicinity of the indole ring of Trp145, which made van der Waals contact the side chain of this amino acid. Tomizawa and Casida have earlier demonstrated that the electron-deficient guanidine moiety of neonicotinoids is likely to contact with the Trp143 [13]. However, the guanidine moiety of Imidacloprid was found to undergo cation-π with the aromatic ring of Trp51 corresponding to Trp53 of Ls-AChBP in fruit fly α1β2 model. Compared with the rat α4β2 model, Trp51 may play an important role in selective insect nAChR-neonicotinoid interactions.

Conclusions

Three-dimensional models of fruit fly $(\alpha1)_2(\beta2)_3$ and rat $(\alpha4)_2(\beta2)_3$ nAChRs were generated by homology modeling and MD simulation. The results showed that the models of fruit fly $(\alpha1)_2(\beta2)_3$ and rat $(\alpha4)_2(\beta2)_3$ nAChRs have a certain validity and practicality. Insecticide Imidacloprid was docked into the putative binding site of fruit fly α1β2 and rat α4β2 nAChRs by Surflex-docking, and the calculated docking energies were in agreement with the experimental results. Docking studies demonstrated that the fruit fly nAChR has greater specificity for Imidacloprid than the rat target-site and revealed that the insect nAChR

Table 3 H-bonds formed between nAChRs and Imidacloprid

Receptor	Atom 1	Atom 2	Distance (Å)	Angle (°)
Fruit fly $(\alpha1)_2(\beta2)_3$nAChR	B/Lys53: amino H	IMI: nitro N	2.437	124.80
	B/Lys53: amino H	IMI: nitro O	2.329	113.41
	B/Glu115: backbone H	H_2O: O	1.661	161.62
	A/Trp145: indole H	IMI: pyridine N	2.889	65.96
	H_2O: H	IMI: pyridine N	2.657	97.56
Rat $(\alpha1)_2(\beta2)_3$ nAChR	A/Tyr191: hydroxyl H	IMI: pyridine N	1.958	98.69
	A/Tyr198: hydroxyl O	IMI: imidazole H	2.742	80.13

loop D plays a key role in the selective interactions of heteromeric nAChRs with Imidacloprid. The results may provide some information for designing highly selective insecticides for controlling insect pests.

References

1. Ortells MO, Lunt GG (1995) Trends Neurosci 18:121–127
2. Lester HA, Dibas MI, Dahan DS, Leite JF, Dougherty DA (2004) Trends Neurosci 27:329–336
3. Brejc K, van Dijk WJ, Klaassen RV, Schuurmans M, van der Oost J, Smit AB, Sixma TK (2001) Nature 411:269–276
4. Karlin A (2002) Nat Rev Neurosci 3:102–114
5. Lloyd GK, Williams M (2000) J Pharmacol Exp Ther 292:461–467
6. Wang H, Yu M, Ochani M, Amella CA, Tanovic M, Susarla S, Li JH, Wang HC, Yang H, Ulloa L, Al-Abed Y, Czura CJ, Tracey KJ (2003) Nature 421:384–388
7. Dani JA (2001) Biol Psychiat 49:166–174
8. Lenoard S, Bertrand D (2001) Nicotine Tob Res 3:203–223
9. Paterson D, Nordberg A (2000) Prog Neurobiol 61:75–111
10. Corringer PJ, Le Novère N, Changeux JP (2000) Annu Rev Pharmacol Toxicol 40:431–458
11. Gotti C, Clementi F (2004) Prog Neurobiol 74:363–396
12. Gundelfinger ED, Schulz R (2000) Insect nicotinic acetylcholine receptors: genes, structure, physiological and pharmacological properties. In: F Clementi, D Fornasari, C Gotti (eds) Handbook of Experimental Pharmacology, vol 144. pp 497–521
13. Tomizawa M, Casida JE (2005) Annu Rev Pharmacol Toxicol 45:247–268
14. Tomizawa M, Casida JE (2003) Annu Rev Entomol 48:339–364
15. Tomizawa M, Millar NS, Casida JE (2005) Insect Biochem Mol Biol 35:1337–1345
16. Perry T, Heckel DG, McKenzie JA, Batterham P (2008) Insect Biochem Mol Biol 38:520–528
17. Bertrand D, Ballivet M, Gomez M, Bertrand S, Phannavong B, Gundelfinger ED (1994) Eur J NeuroSci 6:869–875
18. Lansdell SJ, Millar NS (2000) Neuropharmacology 39:671–679
19. Lansdell SJ, Millar NS (2004) J Neurochem 90:479–489
20. Chamaon K, Schulz R, Smalla KH, Seidel B, Gundelfinger ED (2000) FEBS Lett 482:189–192
21. Chamaon K, Smalla KH, Thomas U, Gundelfinger ED (2002) J Neurochem 80:149–157
22. Huang Y, Williamson MS, Devonshire AL, Windass JD, Lansdell SJ, Millar NS (1999) J Neurochem 73:380–389
23. Wiesenr P, Kayser H (2000) J Biochem Mol Toxicol 14:221–230
24. Tomizawa M, Casida JE (2001) Pest Manag Sci 57:914–922
25. Ihara M, Okajima T, Yamashita A, Oda T, Hirata K, Nishiwaki H, Morimoto T, Akamatsu M, Ashikawa Y, Kuroda S, Mega R, Kuramitsu S, Sattelle DB, Matsuda K (2008) Invert Neurosci 8:71–81
26. Lindstrom JM (2003) Ann N Y Acad Sci 998:41–52
27. Sine SM (1993) Proc Natl Acad Sci USA 90:9436–9440
28. Kao PN, Karlin A (1986) J Biol Chem 261:8085–8088
29. Dellisanti CD, Yao Y, Stroud JC, Wang ZZ, Chen L (2007) Nat Neurosci 10:953–962
30. Unwin N (2005) J Mol Biol 34:967–989
31. Miyazawa A, Fujiyoshi Y, Unwin N (2003) Nature 423:949–955
32. Smit AB, Syed NI, Schaap D, van Minnen J, Klumperman J, Kits KS, Lodder H, van der Schors RC, van Elk R, Sorgedrager B, Brejc K, Sixma TK, Geraerts WPM (2001) Nature 411:261–268
33. Hansen SB, Talley TT, Radic Z, Taylor P (2004) J Biol Chem 279:24197–24202
34. Celie PHN, Klaassen RV, van Rossum-Fikkert SE, van Elk R, van Nierop P, Smit AB, Sixma TK (2005) J Biol Chem 280:26457–26466
35. Talley TT, Harel M, Hibbs RE, Radic Z, Tomizawa M, Casida JE, Taylor P (2008) Proc Natl Acad Sci USA 105:7606–7611
36. Hansen SB, Taylor P (2007) J Mol Biol 369:895–901
37. Celie PHN, van Rossum-Fikkert SE, van Dijk WJ, Brejc K, Smit AB, Sixma TK (2004) Neuron 41:907–914
38. Hansen SB, Sulzenbacher G, Huxford T, Marchot P, Taylor P, Bourne Y (2005) EMBO J 24:3635–3646
39. Brown LA, Ihara M, Buckingham SD, Matsuda K, Sattelle DB (2006) J Neurochem 99:608–615
40. Matsuda K, Buckingham SD, Kleier D, Rauh JJ, Grauso M, Sattelle DB (2001) Trends Pharmacol Sci 22:573–580
41. Buckingham SD, Lapied B, Corronc HL, Grolleau F, Sattelle DB (1997) J Exp Biol 200:2685–2692
42. Zhang AG, Kayser H, Maienfisch P, Casida JE (2000) J Neurochem 75:1294–1303
43. SYBYL software, Version 7.3, Tripos Associates Inc, St. Louis, 2006, http://www.tripos.com/
44. Needleman SB, Wunsch CD (1970) J Mol Biol 48:443–453
45. Zhu ZY, Sali A, Blundell TL (1992) Protein Eng 5:43–51
46. Jain AN (2007) J Comput Aided Mol Des 21:281–306
47. Jain AN (1996) J Comput Aided Mol Des 10:427–440
48. Bisson WH, Westera G, Schubiger PA, Scapozza L (2008) J Mol Model 14:891–899
49. Tomizawa M, Lee DL, Casida JE (2000) J Agric Food Chem 48:6016–6024
50. Tomizawa M, Cowan A, Casida JE (2001) Toxicol Appl Pharmacol 177:77–83
51. Shimomura M, Yokota M, Matsuda K, Sattelle DB, Komai K (2004) Neurosci Lett 363:195–198
52. Shimomura M, Yokota M, Ihara M, Sattelle AM, DB MK (2006) Mol Pharmacol 70:1255–1263
53. Ihara M, Shimomura M, Ishida C, Nishiwaki H, Akamatsu M, Sattelle DB, Matsuda K (2007) Invert Neurosci 7:47–51
54. Ohno I, Tomizawa M, Durkin KA, Casida JE, Kagabu S (2009) J Agric Food Chem 57:2436–2440